# Biomechanical simulation of the fetal descent without imposed theoretical trajectory

Romain Buttin, Florence Zara, Behzad Shariat, Tanneguy Redarce, Gilles Grangé

# Biomechanical simulation of the fetal descent without imposed theoretical trajectory

Romain Buttin[a,b], Florence Zara[a], Behzad Shariat[a], Tanneguy Redarce[b], Gilles Grangé[c]

[a] *Université de Lyon, CNRS, Université Lyon 1, LIRIS, SAARA team, UMR5205, F-69622, Villeurbanne, France*
[b] *Université de Lyon, CNRS, INSA de Lyon, Laboratoire Ampère, UMR5005, F-69621, Villeurbanne, France*
[c] *Maternité Port Royal, Groupe Hospitalier Cochin - Saint Vincent De Paul (Assistance Publique - Hôpitaux de Paris), F-75679, Paris, France*

**Abstract**

The medical training concerning childbirth for young obstetricians involves performing real deliveries, under supervision. This medical procedure becomes more complicated when instrumented deliveries requiring the use of forceps or suction cups become necessary. For this reason, the use of a versatile, configurable childbirth simulator, taking into account different anatomical and pathological cases, would provide an important benefit in the training of obstetricians, and improve medical procedures. The production of this type of simulator should be generally based on a computerized birth simulation, enabling the computation of the reproductive organs deformation of the parturient woman and fetal interactions as well as the calculation of efforts produced during the second stage of labor.

In this paper, we present a geometrical and biomechanical modeling of the main parturient's organs involved in the birth process, interacting with the fetus. Instead of searching for absolute precision, we search to find a good compromise between accuracy and model complexity. At this stage, to verify the correctness of our hypothesis, we use finite element analysis because of its reliability, precision and stability. Moreover, our study improves the previous work carried out on childbirth simulators because: (a) our childbirth model takes into account all the major organs involved in birth process, thus potentially enabling different childbirth scenarios; (b) fetal head is not treated as a rigid body and its motion is computed by taking into account realistic boundary conditions, *i.e.* we do not impose a pre-computed fetal trajectory; (c) we take into account the cyclic uterine contractions as well as voluntary efforts produced by the muscles of the abdomen; (d) a slight pressure is added inside the abdomen, representing the residual muscle tone. The next stage of our work will concern the optimization of our numerical resolution approach to obtain interactive time simulation, enabling it to be coupled to our haptic device.

*Keywords:* Biomechanical modeling of organs, Fetal descent, Finite Element model, Medical training.

## 1. Introduction

Traditionally, medical training concerning childbirth for young obstetricians involves performing real deliveries, under supervision. However, this medical procedure becomes more complicated when instrumented deliveries requiring the use of forceps or suction cups become necessary. Thus, the use of learning tools could complement the training of obstetricians (generally considered as too short) and improve the medical procedures. The main objective is to ensure that the obstetrician dares to make the medical gesture needed, to decrease the number of cesareans harming future mothers pregnancies.

Currently many simulators exist. In most common cases, simulators make medical training for instrumented delivery possible using a physical interface. Usually their interface is composed of several physical parts (an assembly of plastic pieces) which represent the anatomy of some organs, generally the pelvis and the head of the fetus. In addition, a motorized articulated system drives these physical parts to simulate the interaction of the fetus with the organs of the parturient woman and the obstetrician. Thus, this haptic device makes it possible to generate resistant forces that reproduce a sensation similar to that felt by the practitioner during delivery. Moreover, these simulators enable the practitioner to increase his experience due to the similarities between the anatomical representation given by plastic parts and reality. Some of these tools permit the simulation of instrumented deliveries using forceps [1]. For example, the Hopkins-designed birth simulator is oriented towards shoulder dystocia [2, 3] and the Noelle$^{TM}$ simulator marketed by Gaumard offers a complete robotized anthropomorphic system including fetal cardiac rhythm [4].

However these dummy tools are not very realistic and it would therefore be interesting to develop a more versatile and configurable tool, making it possible to take into consideration the various anatomical and morphological structures of the fetus and the parturient woman, corresponding to different pathological cases. Such a tool uses Virtual Reality (VR) techniques and is composed of two parts: (1) a computational model part, simulating the birth process; (2) a haptic interface. The implementation of the computerized simulation part could take place through the definition of a complete three-dimensional anatomical representation of the maternal pelvis and the fetus.

In the state of the art [5], there are two types of work: (1) *Pelvic floor simulations* designed to estimate pelvic floor dysfunction and organ prolapse or pelvic floor birth-induced injuries. Usually, these simulations perform a detailed biomechanical model of the levator ani muscles in interaction with

a rigid fetal head during labor; (2) *Birth simulations* based on a simplified biomechanical model of the female reproductive system and the fetus. In these simulations, expulsive forces are approximated by imposing kinematic boundary conditions on the fetal head, imitating reality.

Unfortunately, the *pelvic floor simulations* based on biomechanical models aim to create complex and accurate models, at the expense of a long computation time. Moreover, they do not take all the relevant pelvic organs involved in the birth process into consideration. On the contrary, the *birth simulations* are simplistic and they do not take proper account of boundary conditions.

Our aim is to develop a versatile birth simulator that offers teaching scenarios at various levels of difficulty and which take into account some complex deliveries. However, we do not seek to obtain an accurate simulation, but rather a convincing one. In order to fulfill our objectives, we propose an approach that lies between the two above-mentioned classes of simulations. It is based on a simplified, but realistic, biomechanical modeling of all the organs involved at the second stage of labor (uterus, abdomen, soft and bony pelvis), allowing the calculation of stresses generated by the descent of the fetus, guided by the cyclic contractions of the uterine and abdominal muscles.

## 2. State of the art

Training simulators are currently used in medicine as an instruction tool or as a medical support for surgery [6, 7, 8, 9, 10]. In the field of obstetrics and gynecology, a large survey of existing medical training simulators has been conducted by Gardner [11, 12] and one more specific to childbirth modeling by Li [5]. Moreover, in 2002 Letterie [13] explored the possible role of Virtual Reality for training in obstetrics and gynecology and concluded that Virtual Reality is a method that is potentially useful for this purpose.

The first Virtual Reality birth simulator was introduced by Boissonnat and Geiger in 1993 [14, 15]. This simulator makes it possible to adjust various geometric parameters such as pelvic organs or fetal morphology. However, this simulator is not equipped with a haptic device and is thus devoid of interaction with the user. It was not designed to train young obstetricians, but rather to establish a prognosis for the delivery by conducting a simulation of the fetal descent guided by a pre-computed imposed trajectory. In 2004, Kheddar [16] developed a simulator coupling a three-dimensional biomechanical model of the fetus and pelvis to a three-axis haptic system representing the hands of the obstetrician. Similarly, Obst [17] proposed a simulator based on biomechanical modeling of the birth process. Here again, as in the previous model, the boundary conditions are not realistic and the simulation is based on an imposed trajectory. Therefore both models are not able to take into account different identified birth scenarios.

On the other hand, many studies have been carried out to determine, as accurately as possible, fetal head deformation or injuries to pelvic floor muscles during the second stage of labor [5]. As previously stated, they do not take into account the entire birth process, but they provide valuable information about the functional and biomechanical aspects of some of the organs involved in the birthing process. Here we present an overview of some of these studies. In 2001, Lapeer [18] presented a non-linear static finite element model of the deformation of a complete fetal skull, subjected to pressures exerted by the cervix during the first stage of labor. This model permits the evaluation of the biomechanics of fetal head molding using a theoretical model of intra-uterine and head-to-cervix pressures. Moreover in 2004, Lapeer presented an augmented reality-based simulation of an obstetric forceps delivery [19]. This simulation is based on a virtual fetus model obtained from MR (Magnetic Resonance) and CT (Computed Tomography) images, and a real forceps delivery tracked with passive optical markers. The contact between the virtual skull and the forceps is then established and visible on the simulator. Then in 2005, he tested the feasibility of a real-time mechanical contact model to describe the interaction between the forceps and the fetal head [20]. It was concluded that an explicit dynamic model to calculate the deformation of the main fetal skull bones only, or a quasi-static model to calculate the deformation of the fetal head in its entirety, can achieve real-time performance.

In addition, Martins [21, 22] studied the simulation of *levator ani* (LA) muscles to observe pelvic floor dysfunctions. A Neo-Hookean constitutive model has been used for the LA muscle. It is considered to be quasi-incompressible and isotropic with a single fiber direction. The material properties of pelvic floor muscles have been approximated by using data from heart tissues. A realistic model of the fetus, represented by tetrahedral elements, has been used. The fetus is almost undeformable with very high rigidity. By varying maternal and fetal head geometries, as well as some other parameters such as presentation, the maximum muscle stretch ratio has been computed. Recently, Li [23] also investigated the effect of mechanical anisotropy on the biomechanical response of the LA muscle during childbirth. He varied the relative rigidity between the fiber and the matrix components, whilst maintaining the same overall stress-strain response in the direction of the fiber. Thus, a fetal skull was passed through two pelvic floor models, which incorporate the LA muscle with different anisotropy ratios. Interactions between the LA muscle and the fetal skull were modeled during the second stage of labor using finite deformation elasticity and frictionless contact mechanics. Results showed a substantial decrease in the magnitude of the force required for delivery as the fiber anisotropy was increased.

Furthermore, Mizrahi and Karni [24] have presented a mechanical model of the uterus using a kinematic approach. The expression of the strain gradients and strain compatibility for the middle surface of the uterus shell in curvilinear-oblique coordinate networks are produced. As boundary conditions, they considered that the displacements of the cervix are zero in a single contraction and remain constant during the second stage of labor when the cervix is fully dilated. Moreover, they assumed the volume bounded by the organ to be constant during the deformation, due to the incompressibility of the inter-uterine fluid. They also presented a study to improve the anisotropic behavior of the uterine muscle [25].

Contrary to these precision driven approaches, our work aims to represent realistic material properties and boundary conditions for all the organs involved in the second stage of labor [26]. Moreover, our aim is to maintain a balance between accuracy and computational complexity. For this reason, our biomechanical and geometric models have been simplified to reduce the overall computation cost.

## 3. Our model of the second stage of labor

Delivery is a complex physiological phenomenon involving many organs. It must be remembered that the embryo develops during gestation in the uterus. Then, during the three stages of labor, the uterine contractions combine with the forces of the abdomen and diaphragm to expel the fetus. The second stage of labor starts at full dilatation of the cervix until the birth of the baby. During its descent, the fetus will cross the pelvic inlet (superior pelvic strait) and the pelvic outlet (inferior pelvic strait). Consequently, the head of the fetus which is the widest part, will deform the pelvic floor muscles to extricate itself from the utero-vaginal canal. Note that for our simulation, we consider the most common head presentation, *e.g.* the occiput anterior (OA) presentation.

### *3.1. Selection of organs to model*

Many organs are involved during the second stage of labor. To simplify our model, we considered only the essential components, that is to say the uterus, abdomen and soft and bony pelvis, as well as the fetus. We have not modeled the placenta, the bladder and the rectum:

- The placenta is a relatively thin body which is located inside the uterine pocket. Mechanically, this body causes only a partial increase in the thickness of the uterine wall. It is released a few minutes after the fetal exit, during the third stage of labor known as "delivery of the placenta". But, as we focused only on the second stage of labor, we do not have to integrate it into our model.

- The bladder is rather imposing because it may contain about 350 ml of liquid. However, at the beginning of labor it is emptied, significantly reducing its size and limiting its effect on the simulation of organ motion. Therefore, this body has not been integrated into our model.

- In the same way, the rectum does not have an important role during labor, and modeling it does not represent a real contribution to the accuracy of the results.

### *3.2. Generation of organs mesh*

The geometry of the various organs has been extracted from MRI data for soft tissues and CT-scan data for the bony parts of pregnant women. The resolution of MRI data is 5 mm (the distance between MRI sections). The bony pelvis was obtained from high precision scanner data (2 mm). To retrieve organs geometry, these data have been segmented using ITK SNAP software resulting in very dense meshes. Consequently, to decrease the computation time, the number of mesh vertices should be reduced. To achieve the above simplification requirements, we used the ReMESH [27] software that use angular gradient method. For example, Fig. 1 shows the left wing of the pelvis before its simplification (1,750,000 nodes) and after simplification (3,500 nodes), and clearly the details of the bony section composed of the left and right iliac wings as well as sacro-lumbar spine is preserved.

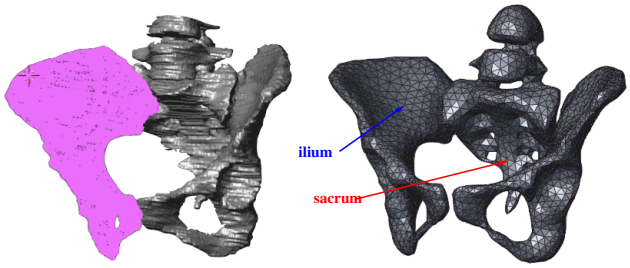


Figure 1: Pelvis meshing: (left) before simplification (1,750,000 nodes), (right) after simplification (3,500 nodes).

This step allows us to reduce approximately 95% of the elements. However, it is important to find a compromise between mesh simplification and simulation time on one hand, and the conservation of some morphological details, on the other hand. Consequently, we verified the impact of our simplification strategy on the geometrical precision of our mesh.

For this, we used the MESH software [28] which permits to compute the average distance $d_{mean}$ between the initial and simplified meshes for different mesh simplification rates. However, this average distance is a global value, but we seek to evaluate the preservation of some anatomical details in modeled organs. Consequently, we have defined a metric for each given organ (called characteristic and denoted $d_{organ}$) to determine a precision parameter (denoted $\alpha$), defined by:

$$\alpha = 100 \times \frac{d_{organ} - d_{mean}}{d_{organ}}.$$

This coefficient (dimensionless) provides an estimation of the error. Thus, $\alpha$ has been calculated for each organ to take into account the most critical case. Indeed, more the value of $d_{organ}$ is high, more the influence of $d_{mean}$ will be negleted. We therefore took relatively small characteristic quantities: for the pelvis, the thickness of the iliac wing; for the uterus, the uterine membrane thickness; and for the fetus, the diameter of the fetal head. Consequently, we determined the above precision parameter for these organs, for mesh simplification rates varying from 10% to 98%. Fig. 2 shows the evolution of the mesh precision parameter $\alpha$ in function of mesh simplification rate, for each organ.

We note that for up to 90% of node decimation, the mesh conserves a precision higher than 85%. This simplification is consistent with the requirements of our application [26]. Fig. 3 shows the distance map between the original mesh and a mesh simplified to 90% for the fetus. Also, we note that the error lies between 4 and 7 mm. A fetus measuring approximately 30 cm long, this represents an error of less than 2%.

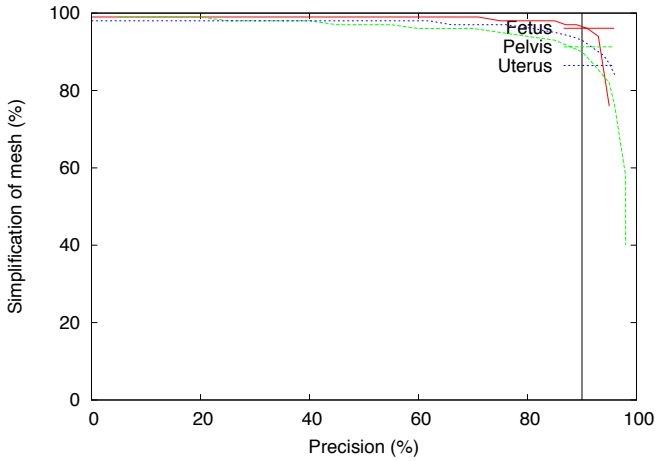


Figure 2: Comparison of the evolution of precision of the pelvis mesh (green), fetus (red), and uterus (blue) in function of the mesh simplification rate.

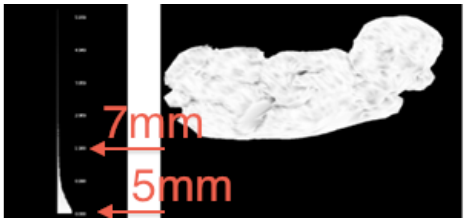


Figure 3: Distance map between the original and the simplified mesh of the fetus to 90% with an error estimation lies between 4 to 7 mm.

At the end, this simplification step permits to obtain the external mesh of the organs to be modeled and Table 1 shows the number of nodes before and after the simplification step for the considered organs.

| | Number of mesh nodes | |
|---|---|---|
| | Before simplification | After simplification |
| Pelvis | 1,750,000 | 3,500 |
| Fetus | 21,500 | 2,800 |
| Abdomen | 38,863 | 3,268 |
| Uterus | 42,811 | 2,348 |

Table 1: Number of mesh nodes before and after the simplification step.

But, since we wish to model the 3D deformation behavior of organs, these surface meshes should then be converted into volume meshes. Consequently, we used the Abaqus FE software developed by Dassault System, with the *tetrahedralization* algorithm based on the Delaunay technique, commonly used in Computer Graphics [29, 30].

### 3.3. Computational model

In this section, we briefly present the computational models used in our work. These concern the study of constitutive equations that connect applied stresses to body deformations, as well as the biomechanical parameters and assumptions about the involved organs.

*Constitutive equations.* Hooke's law allows the modeling of linear elastic behavior. For homogenous and isotropic materials, it is defined by:

$$\sigma = D \cdot \epsilon$$

with $\sigma, \epsilon$ the stress and strain tensors, and $D$ defined by

$$[D] = \begin{bmatrix} \lambda+2\mu & \lambda & \lambda & 0 & 0 & 0 \\ \lambda & \lambda+2\mu & \lambda & 0 & 0 & 0 \\ \lambda & \lambda & \lambda+2\mu & 0 & 0 & 0 \\ 0 & 0 & 0 & \mu & 0 & 0 \\ 0 & 0 & 0 & 0 & \mu & 0 \\ 0 & 0 & 0 & 0 & 0 & \mu \end{bmatrix},$$

with $\lambda$ being the Lame first parameter and $\mu$ the shear modulus defined by

$$\lambda = \frac{E\,\nu}{(1+\nu)\,(1-2\nu)},\ \mu = \frac{E}{2\,(1+\nu)},$$

with $E$ being the Young modulus and $\nu$ the Poisson ratio of the material.

For the modeling of an incompressible hyper-elastic behavior, the Mooney-Rivlin model fits better the experimental data than Neo-Hooke's law, but requires an additional empirical constant. As the high precision is not our priority and because of the inherent difficulties in obtaining *in vivo* data, the introduction of an additional parameter will probably not improve the results. For this reason, we choose Neo-Hooke's law, for the incompressible hyper-elastic behavior modeling, characterized by a function of strain energy $W$, depending only on the current state of the deformation with $\sigma = \frac{\partial W}{\partial \epsilon}$. The strain energy per unit of reference volume is defined by:

$$W = C_{10}\,(\overline{I_1} - 3),$$

with $C_{10} = \frac{1}{2}\,G$, and $G = \frac{E}{2(1+\nu)}$ the shear modulus, and $\overline{I_1}$ the first deviatoric strain invariant defined as $\overline{I_1} = \overline{\lambda_1}^2 + \overline{\lambda_2}^2 + \overline{\lambda_3}^2$ with $\overline{\lambda_i}$ the deviatoric stretches defined by $\overline{\lambda_i} = J^{-\frac{1}{3}}\lambda_i$, where $J$ is the total volume ratio and $\lambda_i$ are the principal stretches.

*Mechanical properties.* The main difficulty in using these constitutive laws remains the choice of appropriate values for these biomechanical parameters ($E$, $\nu$ and $C10$). Indeed, the exact values are extremely difficult to determine and may vary by one or several order of magnitude, depending on the protocol used for their estimation. Moreover, the values obtained *in vitro* are usually inappropriate, and it is often difficult to perform the experiments *in vivo*.

For example, Mazza *et al.* [31] present a study performed with an aspiration device to characterize the mechanical properties of human uterine cervices *in vivo*. The average values of the stiffness parameter vary from 0.095 to 0.24 bar/mm, for experiments on eight patients, aged from 47 to 69 years and having had 1 to 4 births. However, it is difficult to use these values obtained in non-pregnant women because of the significant changes in mechanical properties during pregnancy [32]. For this reason, Bauer *et al.* [33] present another study performed

with the same device but on pregnant women (between 21 and 36 weeks' gestation). They obtained stiffness values between 0.013 and 0.068 bar/mm - non-pregnant tissue was significantly stiffer than pregnant tissue in both tension and compression. In our work the mechanical parameters $C10$, $\nu$ and $E$ have been set at the values found in [32] and [34].

### *3.4. Biomechanical model of organs*

In this paragraph, we introduce the biomechanical behavior and parameters, as well as the boundary conditions of the selected organs modeled in our simulation illustrated in Fig. 4.

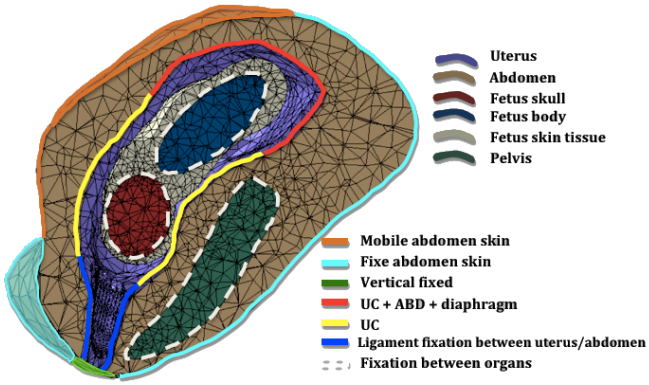


Figure 4: Summary diagram of modeled organs and their boundary conditions. *ABD: abdominal forces.*

*Pelvis.* The bony pelvis is composed of three bones: the left and right iliac wings, and sacro-lumbar spine. These bones are connected to each other by the muscular section of the pelvis, by a set of ligaments. This network of perineal muscles in the pelvis, located at the pelvic outlet, is commonly called "pelvic floor". The bony pelvis plays an important role during the childbirth, by guiding the fetal head into the birth canal by performing a movement called "nutation", composed of two dependent rotations: a forward tilting of the sacrum when the fetal head is introduced into the vaginal canal, and an abduction movement of the iliac wings resulting in a decrease in the promonto-retropubic diameter as well as an increase of the sub-sacra-pubic diameter. The pelvic floor behaves as an elastic manner and can undergo large deformations.

Although slight movements occur at both wings of the bony pelvis, the main moving part of the spine and pelvis is the coccyx. For the ease of the computation, the abduction movement has been neglected, and the pelvic floor has been incorporated into the abdomen model of the parturient woman. Consequently, we have considered the iliac wings of the bony pelvis to be stationary and undeformable, the upper sacro-lumbar spine to be fixed, and we have only allowed a rocking motion at the lower sacro-lumber spine.

For the mechanical behavior, Fung [32] recalls experiments performed by Yamada [35] suggesting that Hooke's law is applicable to bones for a limited range of strains. Therfore, we used the Hooke's law model for the bony pelvis that enables small deformations. For the Young modulus of the bone, Dufour and Pillu [34] presented an average value from 15 to 19 MPa. This average value includes the trabecular and cortical parts of the bone. Cortical bone being much denser than trabecular bone (the spongy part of the bone), we chose a Young modulus $E = 23$ MPa to focus on the cortical bone. The Poisson ratio for bone is between 0.2 and 0.3 [36], and we chose $\nu = 0.3$ for the Poisson ratio of the bony pelvis. Moreover, we estimated the density value at $1,000$ kg/m3.

*Abdomen.* As previously explained, we incorporated the pelvic floor into the abdomen model. Thus, we provided mechanical behavior for the abdomen close to that for the muscular pelvic tissues, *i.e.* elastic and compressible. These properties enable the repositioning of the constituent elements during the descent of the fetus. Finally, the abdomen was modeled as a hyperelastic material using the Neo-Hooke constitutive law with a density of 2,500 kg/m3 and $C10 = 5$ kPa.

Let's now consider the boundary conditions. During labor and delivery, the parturient's back is immobilized by the birth chair. The fetal head preventing the closing of the coxal-femoral angle, parturient's thighs can be considered fixed during delivery. The moving parts of the external surface of the abdomen are then: (1) the front face that will be gradually deflated as the fetus moves forward; (2) the external portion of the vulva which should be removed in order to allow the fetal head to be extracted. As the fetal head is much larger than the utero-vaginal canal, the generated forces would tend to push the muscular tissues down. This is limited by the skin resistance which is one of its most interesting properties in our context. As we do not model the skin, we prevented the organs prolapse by imposing a limit condition to the vaginal canal elements by only permitting their movement in the horizontal plane. Vertical displacements (Inferior-superior) of the vagina are considered to be null (see Fig. 5).

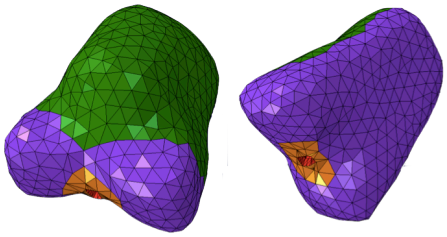

Figure 5: Boundary conditions for the abdomen model: (purple) the fixed parts; (orange) the vulva can be stretched; (red) vaginal area vertically blocked; (green) all displacements permitted.

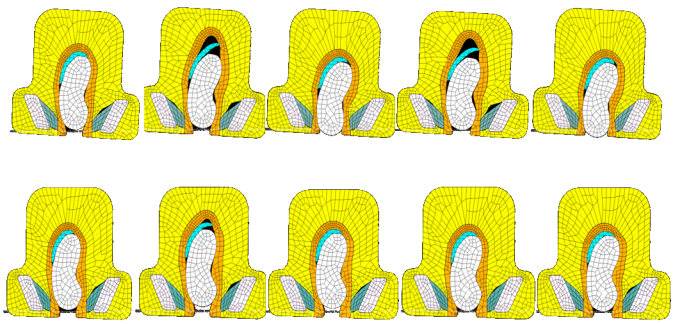

Figure 6: 2D cuts in the coronal plane of different stages of childbirth without (top) or with (bottom) internal pressure. Fetus (white), pelvic muscles (green), uterus (orange), pelvis (gray), placenta (blue), abdomen (yellow).

Moreover, to retain cohesion between the uterus, pelvis and fetus inside the abdomen, we added a slight pressure of 9,500 Pa representing the residual muscle tone. Fig. 6 illustrates it in 2D.

*Uterus.* The uterus is a thin closed shell membrane in which the fetus develops during pregnancy. During labor, the uterus is the most important organ in the pelvic system since it supports all the efforts applied by other organs. Moreover during the second stage of labor, the uterus exerts a pressure on the fetus, pushing it into the birth canal. The inner walls of the uterus are flattened against the body of the fetus, decreasing the uterine volume throughout the descent, until the muscular membrane forms only a small clot in the perineal area. Finally, its height is approximately one third of its original height.

The work of Mizrahi showed that the behavior of uterine muscles changed during the childbirth, with an isotropic behavior in the early stages of childbirth and an anisotropic one with the progress of labor [25]. To simplify our model, we consider an anisotropic behavior for the uterine membrane. So the uterus has been modeled as a Neo-Hookean material with a density of 950 kg/m3 and $C10 = 30$ kPa [31, 33].

As boundary conditions, the displacements of the vaginal canal are limited in the transverse plane to allow the opening and closing of the vaginal canal, avoiding descent of the organs. Moreover, the uterus is composed of a series of tendons allowing it to be fixed to the bony pelvis. Consequently, we connected the displacement field in the lower part of the uterus to the pelvis, as shown in red in Fig. 10.

For the contacts, the uterus is the interface between the maternal abdomen and the fetus, which implies that the thrust and fetal movement will occur through to the uterus. At the end, contacts between the uterus and other organs can be divided into three groups:

- Uterus - fetus. The contacts between the uterus and the fetus are considered to be frictionless. Indeed, when the labor phase begins, the amniotic fluid drains out of the uterus, but the internal walls are nonetheless fairly well lubricated.
- Uterus - abdomen. The contacts between the uterus and the abdomen are also considered to be frictionless because of the viscous contact between all the organs within the abdomen.
- Uterus - placenta. As stated before, the placenta forms a flattened disk attached to the uterine membrane and remains in contact with the uterus until the end of delivery. From a mechanical point of view, the placenta could be considered as a local over-thickness of the uterine wall, constituting an additional argument to our choice to do not model this organ.

*Fetus.* From the point of view of complexity, it is not possible to model all the organs of the fetus. Therefore, we consider the fetus to be composed of three parts (as shown on Fig. 7):

- The skull. It is considered to be a deformable object as it undergoes significant deformation during delivery.
- The body. It is regarded as an object that is slightly deformable to allow the back of the fetus to move freely and to simulate the global movement.
- The skin tissue. It is considered more elastic than the body and the skull, with a lower elasticity modulus. It should be noted that the skin tissue is the only compressible organ in our model, to reduce the repulsion forces involved by contacts between uterus and fetus.

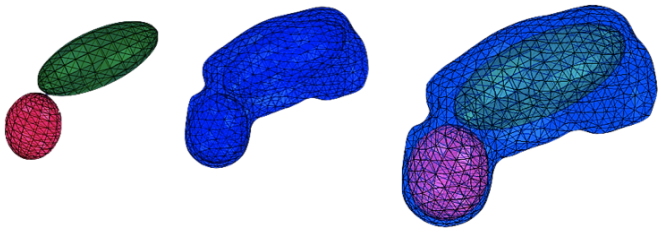

Figure 7: The model fetus is composed of three parts: skull (red), body (green) and skin tissue (blue).

On the same principle as the pelvis and abdomen are attached, the skull and the fetal body are attached to the fetal skin tissue. This imposes a condition to the displacement field of the common nodes of these organs. Therefore, their movements are completely linked, and their displacement field is the same. Consequently the management of contacts in this part of the fetus is not taken into account.

For the mechanical behavior, all the fetus parts were modeled as Neo-Hookean materials with $C10 = 130$ kPa for the skin tissue, $C10 = 75$ kPa for the skull and $C10 = 70$ kPa for the body. Then, assuming that a fetus has a lower muscular density than an adult, we have considered the average fetal density to be slightly lower than 1,000 kg/m3: 400 kg/m3 for the skin tissue and 950 kg/m3 for both the skull and the body. This simplified model preserves the articulation of the skull, induced by the deformation of the skin tissue as shown on Fig. 8.

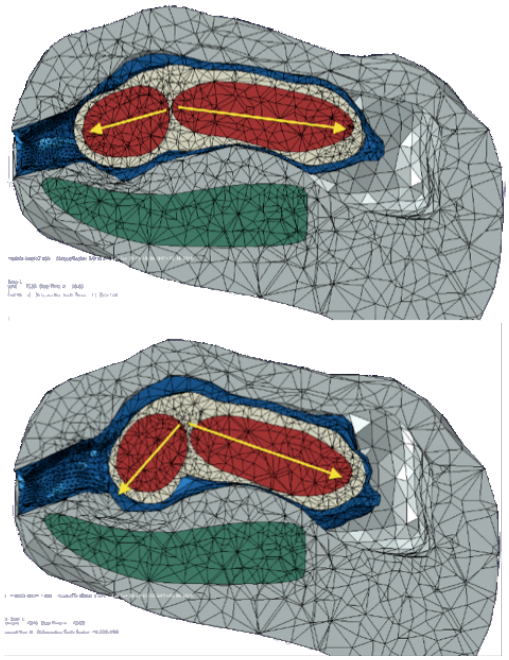

Figure 8: Articulation of the fetal head due to the deformation of skin tissue.

Moreover, during childbirth, the woman is sitting on a chair, in a birthing position called *lithotomy position*. Therefore, the perineal body remains generally horizontal, the fetus is expelled almost horizontally. As the friction between the fetus and uterus are negligible, gravity and therefore the weight of the fetus have small influences on the delivery.

At the end, Table 2 resumes the mechanical properties of the different organs modeled in our simulation.

| | | Constitutive law | Properties |
|---|---|---|---|
| Bony pelvis | | Elastic (Hooke) | Young's modulus = 23 MPa<br>Poisson's ratio = 0.3<br>Density = 1,000 kg/m3 |
| Fetus | skin | Hyperelastic (Neo-Hooke) | $C10$ = 130 kPa<br>Density = 400 kg/m3 |
| | skull | | $C10$ = 75 kPa<br>Density = 950 kg/m3 |
| | body | | $C10$ = 70 kPa<br>Density = 950 kg/m3 |
| Abdomen | | Hyperelastic (Neo-Hooke) | $C10$ = 5 kPa<br>Density = 2,500 kg/m3 |
| Uterus | | Hyperelastic (Neo-Hooke) | $C10$ = 30 kPa<br>Density = 950 kg/m3 |

Table 2: Mechanical properties and constitutive laws of modeled organs.

### *3.5. Uterine contractions and expulsion forces*

We have seen that the uterus is a muscular pouch. Instead of modeling the muscle behavior, we model its consequences *i.e.* the uterine contractions (UC).

These uterine contractions are involuntary and occur 3 or 4 times every ten minutes (one period) [37]. The average duration of a contraction is 90 seconds. Its amplitude varies between "base tonus" (pressure prevailing in the uterus caused by strong deformation) and the intensity of the UC. The true intensity is the difference between these two amplitudes, and corresponds to the effective thrust forces of the uterine contractions during delivery (*cf.* Fig. 9) [37].

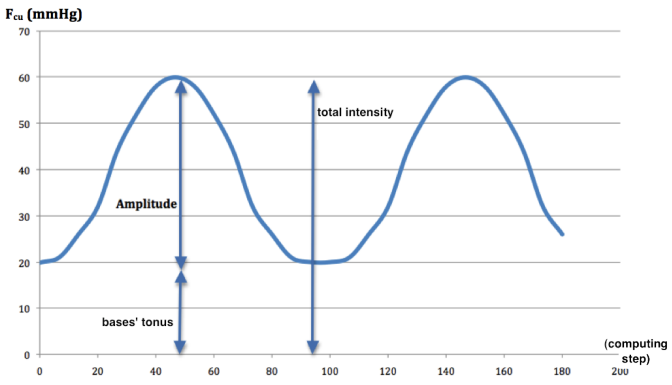


Figure 9: Uterine contraction force (mmHg) *versus* time.

However, this thrust is insufficient to allow the effect of the pelvic muscles to be deleted, and to make the fetal delivery possible. Therefore, during the second stage of labor, the parturient woman must voluntarily produce a series of significant abdominal thrusts synchronized with the uterine contractions. Indeed, even if these forces (called expulsion forces) are about 4 times higher, they have to be added to the UC to exceed the threshold necessary to overcome pelvic floor resistance and expel the fetus.

These expulsion forces are caused by the contraction of the abdominal muscles and the diaphragm. The abdominal muscles are located in the lower abdomen, but they are lifted because of the presence of the fetus. Consequently, they encompass the uterine surface and exert uniform pressure on the top of the uterus. The diaphragm also pushes the fetus toward the vaginal canal.

Finally the descent of the fetus is caused by the combination of the uterine forces and expulsion forces (abdominal and diaphragm forces) applied on the uterus, which shrink the uterine walls causing a force that expels the fetus into the vaginal canal. Fig. 10 is an illustration: in gray, the part of the uterus on which the UCs are applied; in green, the part of the uterus on which the UCs, abdominal and diaphragm forces are applied.

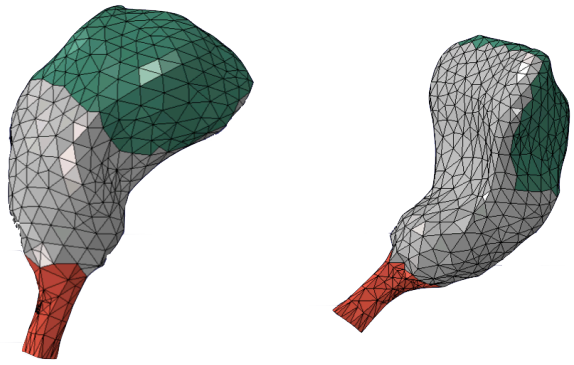

Figure 10: Forces fields applied on uterus: UC (green); UC, abdominal and diaphragm forces (gray).

## 4. Hardware and software specifications

To simulate our biomechanical model, we used Abaqus FE software developed by Dassault Systems, on a Intel PC Core duo, 2.4GHz, 6 GB RAM.

## 5. Results

We used the Euler explicit scheme, with 250 time steps. The duration of our birth simulation is 32 minutes, requiring eight contractions to expel the fetus (with an average fetal head velocity of 0.09 mm/s). The execution time is 45 minutes on our computer specified before.

Fig. 11 illustrates the evolution of the fetus, the uterus and the basin during the simulation. We observe that the fetus moves along the tip of the sacrum expanding the birth canal to make its way out of the womb. We have also included in this article a supplementary color MPEG file which contains several views of the 3D simulation for a better illustration of our 3D simulation results.

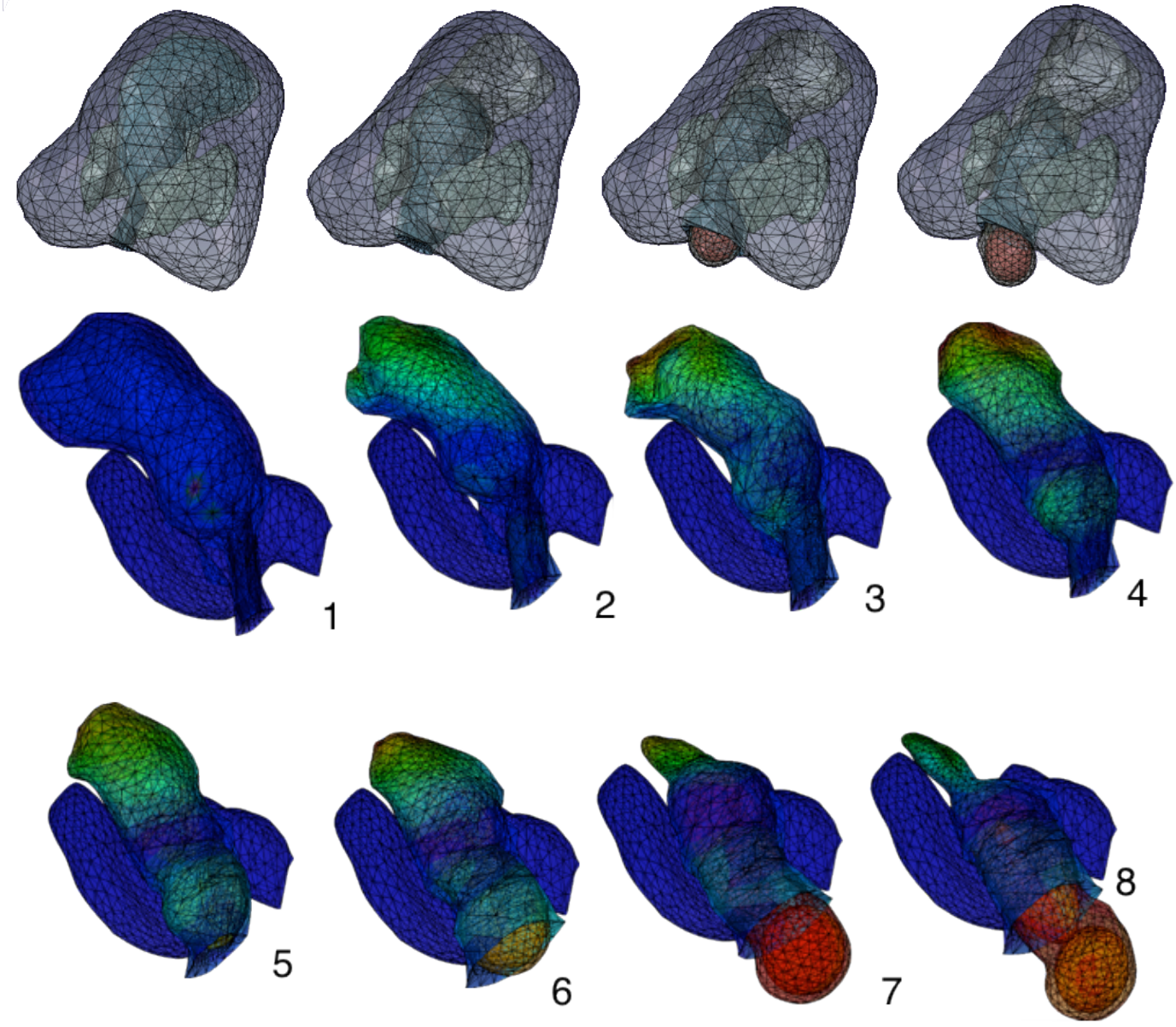


Figure 11: Different phases of the 3D simulation of delivery. The color represents the amplitude of the total displacement.

The validation is a difficult process, because we cannot compare our results with data captured during a real childbirth, due to medical ethics restrictions. However, our medical partners have defined some verification parameters to validate our model: (1) expulsion of the fetus with a correct duration; (2) kinematic behavior of the fetal skull; (3) kinematic behavior of the bony pelvis with the sacrum movement; (4) evolution of the uterus size.

### *5.1. Kinematic behavior of the fetal skull*

We can note that the previous work in the area of birth simulator approximates the uterus and abdomen efforts by kinematic boundary constraints of the fetal head, *i.e* the trajectory of the fetal head is always imposed, while in our work, the kinematic behavior of the fetal skull is computed by the simulation.

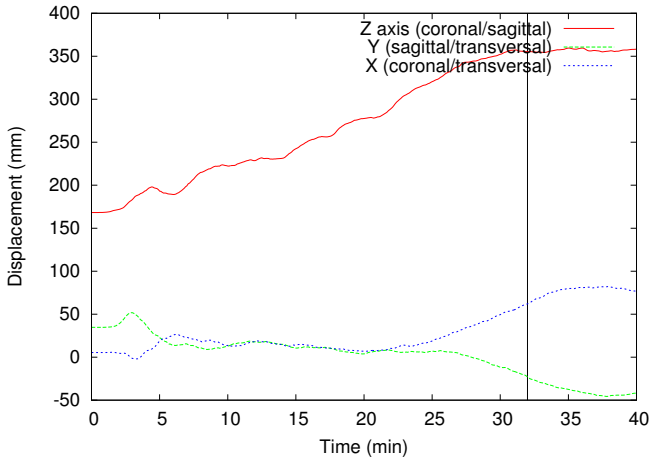


Figure 12: Displacement of the fetal head along the coronal/transversal (X), sagittal/transversal (Y) and coronal/sagittal (Z) axis.

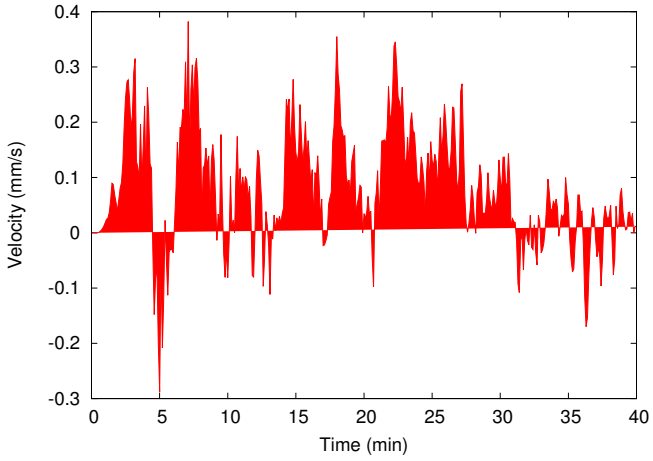


Figure 13: Velocity of the fetal head along the coronal/sagittal (Z) axis.

Fig. 12 shows the 3D evolution of the fetal skull. During the simulation fetal head displacement amplitudes are 51.5 mm along the coronal/transversal axis, 63.5 mm along the sagittal/transversal axis and 184 mm along the coronal/sagittal axis. We can clearly observe that the displacement occurs essentially in the coronal/sagittal axis. If we focus on the kinematic behavior along this latter axis, we can see that the fetal head velocity is not linear. Indeed, the parturient woman does not push continuously, involving increase or decrease in fetal head velocity. When the contractions are no longer sufficient, organs tend to return to their original shape and place and thus to reduce the fetus in the birth canal. This phenomenon is particularly visible if we study the evolution of the velocity of the fetal head along the sagittal/coronal axis (see Fig. 13). The negative velocity indicates the inverse motion of the fetal head.

During its descent, the fetus crosses maternal perineal area, corresponding to a distance of approximately 20 cm. The fetal expulsion phase takes about 30 minutes, which represents statistically an average speed of vertical descent of 0.11 mm/s. With our model, the delivery duration is about 32 minutes. The average speed of the head during the delivery is about 0.09 mm/s. This value is very close to the statistical value.

These results clearly show that the kinematics behavior of the fetal skull is consistent with the reality and provide good indicators of the reliability of our simulation.

### *5.2. Behavior of the uterus*

At the end of a real childbirth, the size of the uterus decreases by approximately 2/3. This can be verified in our model by tracking the front-sagittal trajectory of a point at the top of the uterus over time and comparing it to a point on the lower part of the uterus. In Fig. 14, we can see that the distance between these two points is 230 mm at the beginning of the labor phase and 80 mm at the exit of the fetus. Consequently, we obtain the reduction of about 2/3 in the uterine size, which is consistent with reality.

Moreover, the uterine contractions experienced by the uterus during the second stage of labor involve the reduction in its volume during the descent of the fetus. To verify this behavior, let us consider two points of the uterus chosen in the transversal plane (*cf.* Fig 15). Fig. 16 shows the movement of these two points during the simulation along the coronal/transversal axis. We can see that the displacements follow opposite directions. Consequently, uterine behavior corresponds to uterine contractions.

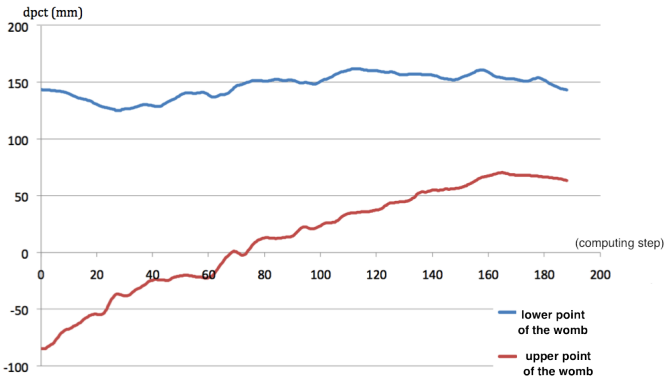


Figure 14: Evolution of the trajectory of a front-sagittal point of the uterus.

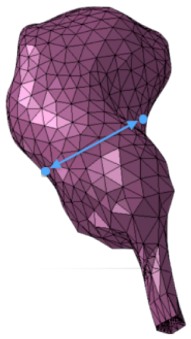

Figure 15: The two points of the uterus followed during the simulation.

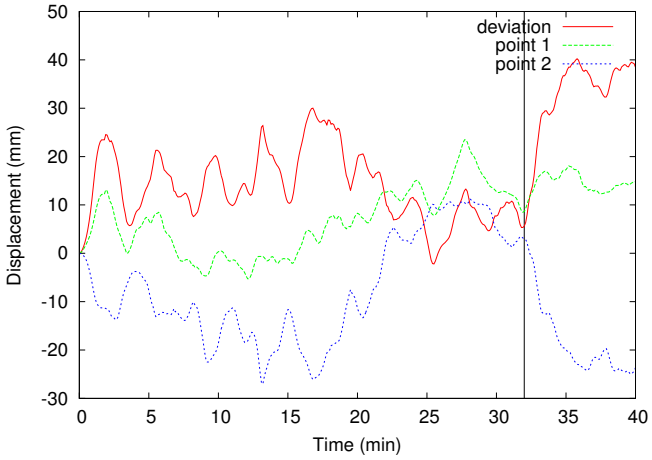


Figure 16: Displacement of two points of the uterus during the simulation.

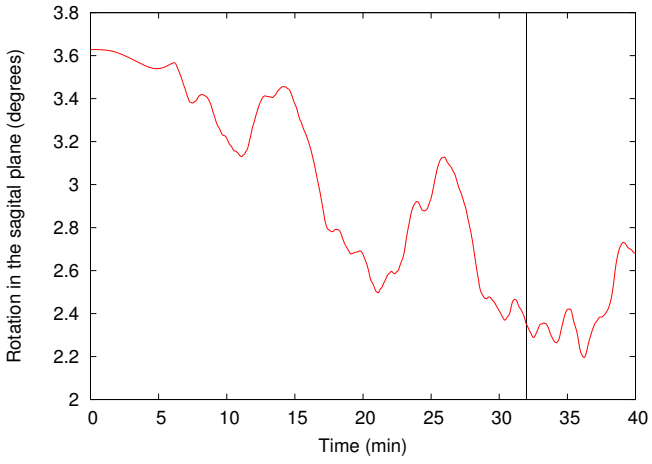


Figure 17: Angular evolution of the pelvis in the sagittal plane.

### 5.3. *Behavior of the bony pelvis*

Let us now consider the behavior of the bony pelvis. Fig. 17 shows its angular evolution in the sagittal plane. We can see two peaks in this curve. The first corresponds to the first contact of fetal head with the sacrum, which is pushed back by the bones of the fetal skull. Then, when the head enters the pelvic outlet, the second peak is caused by the passage of the rest of the body of the fetus. Moreover, as in reality, we can note that at the end of labor (32 minutes later), the pelvis does not return to its initial position.

### 5.4. *Behavior of the fetal head*

Fig. 18 shows the deformation of the head during the simulation. This deformation is caused by the compression of the skull by the pelvic muscles. Even if we did not model the head using a plastic law, our hyper-elastic model enables this deformation during the descent of the fetus enhancing the realism of the simulation.

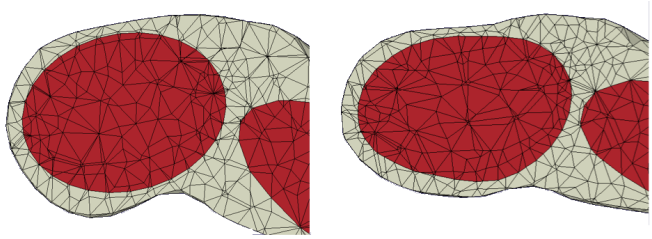

Figure 18: Light crushing of the fetal head during the simulation.

### 5.5. *Integration in the BirthSIM haptic simulator*

We integrated our results in the BirthSIM [38, 39, 40] physical simulator (see Fig. 19), by inputting the fetal head position computed by our simulation. The haptic device reproduced satisfactorily the descent of the head. To illustrate this result, we include in this paper a supplementary color MPEG file which shows both the biomechanical simulation and the use of its results in the BirthSIM device.

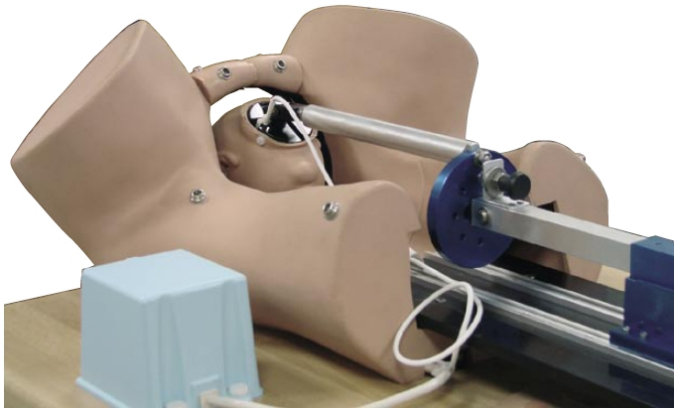

Figure 19: The BirthSIM simulator composed of two sections: a mechanical section and an electro-pneumatic section.

As illustrated in Fig. 20, our computed trajectory (in green) has been compared with the imposed fetal head skull trajectory used by BirthSIM simulator (in red). The BirthSIM model does not take the anatomic reality into account for fetal head acceleration variations and the displacement of the fetus is supposed linear and cyclic (in red). For this reason, we can see that the main difference between the two trajectories appears when the fetal head leaves the pelvic floor (before 15 minutes). We can also see that both models converge almost at the same maximum amplitude.

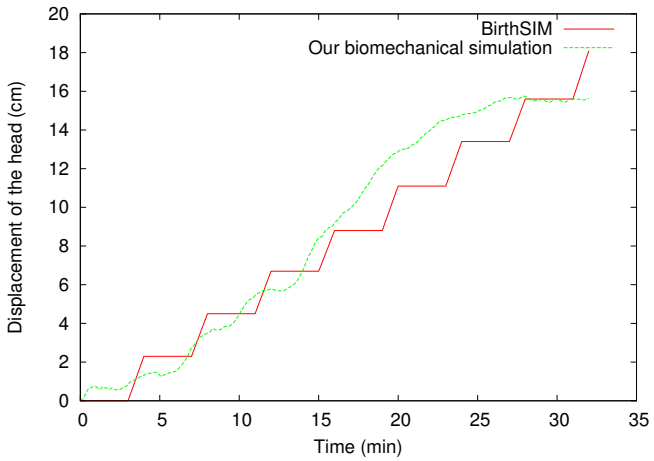


Figure 20: Comparison between the BirthSIM trajectory of the fetal head with that obtained with our model.

Hence, our study still makes it possible to produce new trajectories that can be reproduced by BirthSIM, increasing its realism in the teaching of young obstetricians. Moreover, our aim is to put these trajectories in a simulator integrating 6 degrees of freedom to use all the benefit of the simulation.

## 6. Mode of availability of the system software

Details on the software (Abaqus project) can be obtained from the author by sending a letter of request.

## 7. Discussion and conclusion

In this paper, we presented a biomechanical modeling of interactions between the fetus and the parturient woman. Unlike all the existing Virtual Reality simulators that impose a precomputed trajectory [14, 16], our biomechanical model allows a realistic simulation of the descent of the fetus through the birth canal during the second stage of labor. This simulation, taking into account the morphology of the organs, enables the computation of the real trajectory of the fetus.

To decrease the simulation computation time, we have only considered the main organs involved in childbirth: fetus, uterus, abdomen and pelvis. The geometrical model of the organs is obtained by processing medical image data (CT-scan and MRI) of women close to delivery. Moreover, the simulation is based on the principles of continuum mechanics and uses the finite element method.

The biomechanical model of the fetus is composed of three elements: the skin tissue, the body and the skull. The hyperelastic law of Neo-Hooke has been used to simulate the fetus, abdomen and uterus of the parturient woman, and the elastic law of Hooke has been used to simulate the pelvis. Then, the uterine contractions and expulsion forces (abdominal and diaphragm forces) were modeled as three force fields applied on different parts of the uterus, involving the descent of the fetus in the birth canal. Note that an additional force field has been added to simulate the constant pressure inside the body of the parturient woman.

The quantitative validation is very difficult because we cannot compare our results with medical image acquisitions of a real childbirth, due to medical ethics restrictions. Consequently, we tried to verify the global behavior of the model by examining some characteristic features. The obstetricians of St Vincent de Paul Hospital, in Paris (Doctor G. Grangé and Professor C. Adamsbaum) have determined some validation features (behavior of the tip of the sacrum, decreasing of the uterus size, behavior of the bony pelvis, etc.). The quantitative comparisons with reality show that our model behaves quite well. Moreover, the trajectory computed during the simulation could improve an existing haptic device [38, 39] used for teaching young obstetricians.

This first work allowed us to verify the feasibility of such a model. However, we can note that the simplification made for the organs modeling and simulation, as well as for the contractions, does not allow simulating with high precision the cardinal movements of the fetus during its descent. We have now to quantify with our medical partners, the tradeoff between the accuracy of the simulation, and the aims of the simulator. Indeed, for the restitution of the sensibility of the gesture, it may not be necessary to simulate all the delivery with a high level of precision. Furthermore, some complementary work focuses only on the damage made on the pelvic floor muscles during vaginal delivery [21] have to be considered to ameliorate our simulator.

The next step for the simulation is to achieve interactive execution time, using GPU, to couple our biomechanical simulation to a haptic device. Indeed, our final aim is to obtain a real training system in collaboration with educational software specialists. In this context, we plan to use the Open Source Framework SOFA (http://www.sofa-framework.org) [41, 42] with some previous results already obtained using the tensor-mass model [43]. Moreover, we have to communicate the forces, generated by the simulation, to the haptic device. These forces will have to be validated and we may have to use an implicit integration scheme to ensure their values are correct.

## Acknowledgment

This work is partly financed by a grant from the GMCAO project of the ISLE cluster of the French Rhône-Alpes region. Special thanks to Jérémie Anquez (TELECOM ParisTech, CNRS, UMR-5141, LTCI) for the segmentation of the medical data provided by Prof. Catherine Adamsbaum (St Vincent de Paul Hospital (AP-HP), Paris).

## Conflict of interest statement

We declare that we have no conflicts of interest.

## References


[1] R. Moreau, M.-T. Pham, R. Silveira, T. Redarce, X. Brun, O.Dupuis, Design of a new instrumented forceps: Application to safe obstetrical forceps blade placement, IEEE Transactions on Biomedical Engineering 7 (2007).

[2] E. J. Kim, P. Theprungsirikul, M. K. McDonald, E. D. Gurewithsch, R. H. Allen, A biofidelic birthing simulator, IEEE Engineering in Medicine and Biology Magazine 24 (2005) 34–39.

[3] R. H. Allen, On the mechanical aspects of shoulder dystocia and birth injury, Clinical obstetrics and gynecology 50(3) (2007) 607623.

[4] J. S. Eggert, M. S. Eggert, P. Vallejo, Interactive education system for teaching patient care. patent no. us2003/0081968a1, 2003.

[5] X. Li, J. A. Kruger, P. Nash, M. Nielsen, Modeling childbirth: elucidating the mechanisms of labor, Wiley Interdisciplinary Reviews: Systems Biology and Medicine 2 (2010) 460–470.

[6] D. Aulignac, C. Laugier, J. Troccaz, S. Vieira, Towards a realistic echographic simulator, Medical Image Analysis 10 (2006) 71–81.

[7] H. K. Cakmak, Advanced Surgical Training in Laparoscopy with VEST Simulators, in: 2eme Worshop on Basic Anatomy and advanced Technology in Laparoscopic Surgery, Kiel Allemagne.

[8] S. Cotin, H. Delingette, J.-M. Clement, V. Tasseti, J. Marescaux, N. Ayache, Volumetric deformable models for simulation of laparoscopic surgery, in: International Symposium on Computer and communication Systems for Image Guided Diagnosis and Therapy, Computer Assisted Radiology, Paris, France.

[9] P. Dubois, J.-F. Rouland, P. Meseure, S. Karpf, C. Chaillou, Simulator for laser photocoagulation in ophtalmology, IEEE Transaction in Biomedical Engineering 42 (1995).

[10] P.-Y. Zambelli, C. Bregand, S. Dewarrat, G. Marti, C. Baur, P. Leyvraz, Planning and navigation solution in resurfacing hips surgery: a way to reduce the surgical approach, in: Poster session, 3rd Annual meeting of the International Society Orthopaedic Surgery, Marbella, Spain.

[11] R. Gardner, Simulation and simulator technology in obstetrics: past, present and future, Expert Review in Obstetrics & Gynecology 2 (2007) 775–90.

[12] R. Gardner, D. B. Raemer, Simulation in obstetrics and gynecology, Obstetrics and gynecology clinics of North America 35 (2008) 97–127.

[13] G. Letterie, How virtual reality may enhance training in obstetrics and gynecology, American journal of obstetrics and gynecology 187 (2002) S37–S40.

[14] J.-D. Boissonnat, B. Geiger, 3D simulation of delivery, in: G. M. Nielson, D. Bergeron (Eds.), Visualization 93, IEEE Computer Society Press, San Jose CA, 1993, pp. 416–419.

[15] B. Geiger, Three-dimensional modeling of human organs and its application to diagnosis and surgical planning, Ph.D. thesis, Ecole des Mines de Paris, 1993.

[16] A. Kheddar, C. Devine, M. Brunel, C. Duriez, O. Sidony, Preliminary design of a childbirth simulator haptic feedback, in: IEEE/RSJ, International Conference on Inteligent Robots and Systems, volume 4, pp. 3270–3275.

[17] T. Obst, R. Burghart, E. Ruckhberle, R. Reiner, The delivery simulator: A new application of medical VT, in: MMVR 2004, Newport Beach, pp. 281–287.

[18] R. J. Lapeer, R. W. Prager, Fetal head moulding: finite element analysis of a fetal skull subjected to uterine pressures during the first stage of labour, Journal of Biomechanics 34 (2001) 1125–1133.

[19] R. J. Lapeer, M. Chen, J. Villagrana, An Augmented Reality based Simulation of Obstetric Forceps Delivery, in: Third IEEE and ACM International Symposium on Mixed and Augmented Reality (ISMAR 2004), pp. 274–275.

[20] R. J. Lapeer, A mechanical contact model for the simulation of obstetric forceps delivery in a virtual/augmented environment, Studies in Health Technology and Informatics 111 (2005) 284–289.

[21] J. Martins, M. Pato, E. Pires, R. Natal-Jorge, M. Parente, T. Mascarenhas, Finite element studies of the deformation of the pelvic floor, Ann N Y Academy of Sciences doi:10.1196/annals.1389.19 (2007) 316–334.

[22] M. Parente, R. N. Jorge, T. Mascarenhas, A. Fernandes, J. Martins, The influence of the material properties on the biomechanical behavior of the pelvic floor muscles during vaginal delivery, Journal of Biomechanics 42 (2009) 1301 – 1306.

[23] X. Li, J. Kruger, M. Nash, P. Nielsen, Anisotropic effects of the levator ani muscle during childbirth, Biomechanics and modeling in mechanobiology (2010).

[24] J. Mizrahi, Z. Karni, A mechanical model for uterine muscle activity during labor and delivery, Israel Journal of Technology 13 (1975) 185–191.

[25] J. Mizrahi, Z. Karni, W. Polishuk, Isotropy and anisotropy of uterine muscle during labor contraction, Journal of Biomechanics 13 (1980) 211–218.

[26] R. Buttin, F. Zara, B. Shariat, T. Redarce, A biomechanical model of the female reproductive system and the fetus for the realization of a childbirth virtual simulator, in: IEEE Engineering in Medicine and Biology Society (EMBC'09).

[27] M. Attene, B. Falcidieno, ReMESH: An interactive environment to edit and repair triangle meshes, in: Shape Modeling and Applications (SMI), pp. 271–276.

[28] N. Aspert, D. Santa-Cruz, T. Ebrahimi, MESH: Measuring errors between surfaces using the hausdorff distance, in: IEEE International Conference on Multimedia and Expo, volume I, pp. 705 – 708.

[29] J.-D. Boissonnat, M. Yvinec, Géométrie algorithmique, ediscience edition, 1995.

[30] D. F. Watson, computing the n-dimensional delaunay-tesselation with application to vorono polytopes, Computer Journal 24 (1981) 167–171.

[31] E. Mazza, A. Nava, M. Bauer, R. Winter, M. Bajka, G. Holzapfel, Mechanical properties of the human uterine cervix: an in vivo study, Medical Image Analysis 10 (2006) 125–136.

[32] Y. Fung, Biomechanics. Mechanical properties of living tissues, Springer, second edition, 1993.

[33] M. Bauer, E. Mazza, M. Jabareen, L. Sultan, M. Bajka, U. Lang, R. Zimmermann, G. Holzapfel, Assessment of the in vivo biomechanical properties of the human uterine cervix in pregnancy using the aspiration test: A feasibility study, European Journal of Obstetrics & Gynecology and Reproductive Biology 144 (2009) S77–S81.

[34] M. Dufour, M. Pillu, Biomécanique fonctionnelle : Membres-Tête-Tronc, Masson, 2007.

[35] H. Yamada, Strength of biological materials, Williams & Wilkins in Baltimore, 1970.

[36] M. Dalstra, R. Huiskes, A. Odgaard, L. Van Erning, Mechanical and textural properties of pelvic trabecular bone, Journal of biomechanics 26 (1993) 523–535.

[37] J.-P. Schaal, D. Riethmuller, R. Maillet, M. Uzan, Mécanique et Technique Obstétricales, sauramps medical, third edition, 2007.

[38] R. Silveira, M.-T. Pham, T. Redarce, M. Btemps, O. Dupuis, A new mechanical birth simulator: BirthSIM, in: IEEE/RSJ International Conference on Intelligent Robots and Systems (IROS'04), Sendai, Japan, pp. 3948–3954.

[39] R. Moreau, Le simulateur BirthSIM : un outil complet pour la formation sans risque en obstétrique, Ph.D. thesis, Institut National des Sciences Appliquées, Lyon, France, 2007.

[40] O. Dupuis, A. Dittmar, G. Delhomme, T. Redarce, M. Betemps, R. Silveira, Simulateur fonctionnel et anatomique daccouchement, 2003. French Licence. Licence Number: 0309569.

[41] J. Allard, S. Cotin, F. Faure, P.-J. Bensoussan, F. Poyer, C. Duriez, H. Delingette, L. Grisoni, Sofa an open source framework for medical simulation, in: MMVR'15, Long Beach, USA.

[42] O. Comas, Z. Taylor, J. Allard, S. Ourselin, Efficient Nonlinear FEM for Soft Tissue Modelling and Its GPU Implementation within the Open Source Framework SOFA, in: ISBMS 2008, London, UK, July 7-8, 2008: proceedings, volume 5104, Springer-Verlag New York Inc, p. 28.

[43] X. Faure, F. Zara, F. Jaillet, J.-M. Moreau, An Implicit Tensor-Mass solver on the GPU for soft bodies simulation, in: Eurographics Workshop on Virtual Reality Interaction and Physical Simulation (VRIPHYS 2012), pp. 1–10.